 doi:10.20944/preprints201710.0096.v1

Article

Multifractal Comparison of Reflectivity and Polarimetric Rainfall Data from C- and X-Band Radars and Respective Hydrological Responses of a Complex Catchment Model

Igor Paz [1,2,*], Bernard Willinger [3], Auguste Gires [1], Laurent Monier [4], Christophe Zobrist [5], Bruno Tisserand [5], Ioulia Tchiguirinskaia [1] and Daniel Schertzer [1]

[1] HMCO, Ecole des Ponts ParisTech, Univ. Paris-Est, Champs-sur-Marne, France; auguste.gires@enpc.fr (A.G.); ioulia.tchiguirinskaia@enpc.fr (I.T.); daniel.schertzer@enpc.fr (D.S.)
[2] Instituto Militar de Engenharia, Rio de Janeiro, Brazil
[3] Veolia Eau Ile-de-France, France; bernard.willinger@veolia.com
[4] Direction Technique et Performance, Veolia, Paris, France; laurent.monier@veolia.com
[5] Veolia Recherche et Innovation, Paris, France; christophe.zobrist@veolia.com (C.Z.); bruno.tisserand@veolia.com (B.T.)
* Correspondence: igor.da-silva-rocha-paz@enpc.fr; Tel.: +33-(0)16-415-3507

Abstract: This paper presents a comparison between rain gauges, C-band and X-band radar data over an instrumented and regulated catchment of the Paris region, as well as their respective hydrological impacts with the help of flow observations and a semi-distributed hydrological model. Both radars confirm the high spatial variability of the rainfall down to their space resolution (respectively one kilometer and 250 m) and therefore underscore limitations of semi-distributed simulations. The use of the polarimetric capacity of the Météo-France C-band radar was limited to corrections of the horizontal reflectivity and its rainfall estimates are adjusted with the help of a rain gauge network. On the contrary, neither calibration was performed for the polarimetric X-band radar of the Ecole des Ponts ParisTech (below called ENPC X-band radar), nor any optimization of its scans. In spite of that and the non-negligible fact that the catchment was much closer to the C-band radar than to the X-band radar (20 km vs. 40 km), the latter seems to perform at least as well as the former, but with a higher scale resolution. This characteristic was best highlighted with the help of a multifractal analysis of the respective radar data, which also shows that the X-band radar was able to pick up a few extremes that were smoothed out by the C-band radar.

Keywords: complex catchment; weather X-band radars; flash floods; multifractals; spatio-temporal variability

1. Introduction

Management of weather extremes– particularly intense precipitation events and heat waves – in Paris area (Île-de-France) is a big challenge for the future. The on-going urbanization and rising population density increase the vulnerability of the region. The adaptation to climate change is a necessity and is now a critical societal issue [1]. The risks and their large associated uncertainties are at odds with people's request for a higher quality of life, as testified by "Grenelle de l'Environnement", COP21 and several European directives. Such life standards require a refined management and control of floods, water and air quality. This could be achieved by our improved abilities to measure, understand, model and predict the hydro-meteorological processes in urban and peri-urban environments. This should be organized over the relevant range of space-time scales and with a much better accuracy and reliability. Conventional local measurements in urban areas often do not satisfy the WMO criteria for measurement of precipitation [2]. Ground-based remote sensing

Preprints (www.preprints.org) | NOT PEER-REVIEWED | Posted: 14 October 2017 doi:10.20944/preprints201710.0096.v1

is becoming more important in elucidating complex structures of urban environment, and the hydro-meteorological challenges become broader and broader [3]. This paper focuses on rainfall and its hydrological consequences on the Bièvre River catchment, approximately 20km from Paris City center. Historically, this catchment is not only known for the severe floods that impact its urban areas, but also for its contribution to Paris floods [4].

Weather radars are the only devices that provide spatio-temporal measurements of rainfall fields. However, as they do not measure rainfall directly, radar based rainfall estimates may have substantial uncertainties. To quantify the uncertainty on accumulated rainfall, the authors usually perform either the inter comparison of different radar products, or compare ground measurements and precipitation estimates on radar pixels where rain gauges are located [5–9]. Tabary [10] shows that in spite of the greatly improved quality of the operational C-band radar estimates, the average differences between the radar estimates (without calibration with gauges) and ground observations vary between 28% and 54%, while increasing with the distance. Polarimetric radars have opened a new perspective to improve estimates for stronger rainfall by using the specific differential phase KDP values to directly estimate the rainfall intensity [8]. However, in the French context, this option remains yet a perspective for the reference operational products of the French meteorological institute Météo-France. Up to now, Météo-France only uses the double polarization for attenuation and clear air corrections. These fact underlines that the optimal choice of radar algorithms remains an open question in the community and therefore a research topic.

The differences of observation scales, and in fact of dimensionality, between radars (typically 1 km) and rain gauges (few tens of cm) add a fundamental complexity to this comparison [7,11,12]. This intrinsic issue of volumetric measurements (radars) vs. point measurement (rain gauges) comparison led to development of other ways of validation of radar products notably hydrological validation. It basically consists in inputting various rainfall fields in hydrological models and checking how it affects their ability to reproduce observed hydrographs. This has been done either in rural [13–16] or urban environment [17–23]. Obviously it has the drawback of relying on imperfect rainfall-runoff models. For instance numerous studies showed a strong influence of rainfall spatio-temporal variability on model response, especially in urban areas where response times are shorter due to high levels of imperviousness and smaller catchments [24–31]. This calls for hydrological models with sufficiently high resolution to properly account for rainfall variability [32]. This is one of the drivers for the development of fully distributed models [22,33–35].

There is also a growing interest for operational hydrological models to fully assess the interest of higher space resolution for the rainfall data. A step in this direction has been made by the SCHAPI ("*Service Central d'Hydrométéorologie et d'Appui à la Prévision des Inondations*", a national service in charge of flood forecasting in France) in the study of Tramblay et al. [36] that compares different Météo-France radar products. Another example can be found in Ochoa-Rodrigues et al. [30] who used nine storm events measured by a dual-polarimetric X-band weather radar at the Cabauw experimental site (Netherlands) to investigate the impact of rainfall input resolution on the outputs of semi-distributed operational hydrodynamic models of seven urban catchments of similar size (between 3 and 8 km^2). The study was carried out in the framework of the RainGain project [37].

The goal of the present study is therefore threefold: (i) a comparison across scales of both C- and X-band radar data using multifractal theory and furthermore enabling the selection of the best X-band radar product for this study; (ii) a hydrological comparison of the rainfall data resulting from C-band radar, X-band radar and rain gauges measurements; (iii) and a study of the impact of increased radar data resolution that enables a better assessment of small-scale rainfall variability. It is carried out over the 110 km^2 upstream catchment of the Bièvre River in the Ile-de-France region. This catchment is an example of a peri-urban area, some parts of which are highly urbanized. Veolia is the company chosen since 1991 by the local authority SIAVB ("*Syndicat Intercommunal pour l'Assainissement de la Vallée de la Bièvre*") to design, install and operate a real time control system of the river over the area. Hence, the study is performed with Veolia's operational model called Optim Sim. Instead of suffering limitations, the aforementioned methodological goal and the present study benefit from cross-fertilization of research and operational hydrology, whereas they have both suffered from a long-lasting divorce [38]. Furthermore, the potential decentralization of meteorological and hydrological data collection, processing and distribution should enable most of businesses to optimize their operational management, because often more than 60% of their activities are weather sensitive.

2. Materials and Methods

This section first presents the experimental catchment in the Paris region that is studied in this paper. It was chosen because of its capacity to generate flash floods upstream to a densely-populated area, especially during strong rainfalls. Obviously due to these features, a strong and efficient regulation had to be implemented throughout the river path. Although enabling to study an operationally challenging area, its makes comparison between simulated and observed hydrography trickier but not impossible. Limitations will be clearly pointed out as well as possible ways of overcoming them. The catchment description is linked with the description of the operational platform and its integrated hydrological model calibrated over the catchment, by explaining their features and the employed methodologies.

Afterward, the details of the selected rainfall events and the available rainfall data of three different types, all of them being used as inputs to the hydrological models, are described. Finally, the differences among the rainfall measuring devices in relation to their geographical locations w.r.t. the catchment, as well as the differences in data processing, and the role of dual-polarization in the rainfall retrieval algorithms are also discussed.

2.1. Case Study Site

The upstream catchment of the Bièvre River is a peri-urban area with a very complex topography in the southwest of Paris region. Two local authorities are in charge of the river system management in the area: the CASQY ("*Communauté d'Agglomération de Saint-Quentin-en-Yvelines*") on the upstream portion and the SIAVB for the downstream portion. Veolia has been given the responsibility to operate the system in this area. A map of the Bièvre River can be found in Figure 1. The river network was plotted with the help of data available for the Ile-de-France region [39]. There are some gaps in this network due to missing data on the storage basins along the Bièvre River and covered parts of the river. The level of urbanization of the catchment increases going downstream (from West to East). The Bièvre River flows in a valley with steep slopes on each side, especially on the northern part.

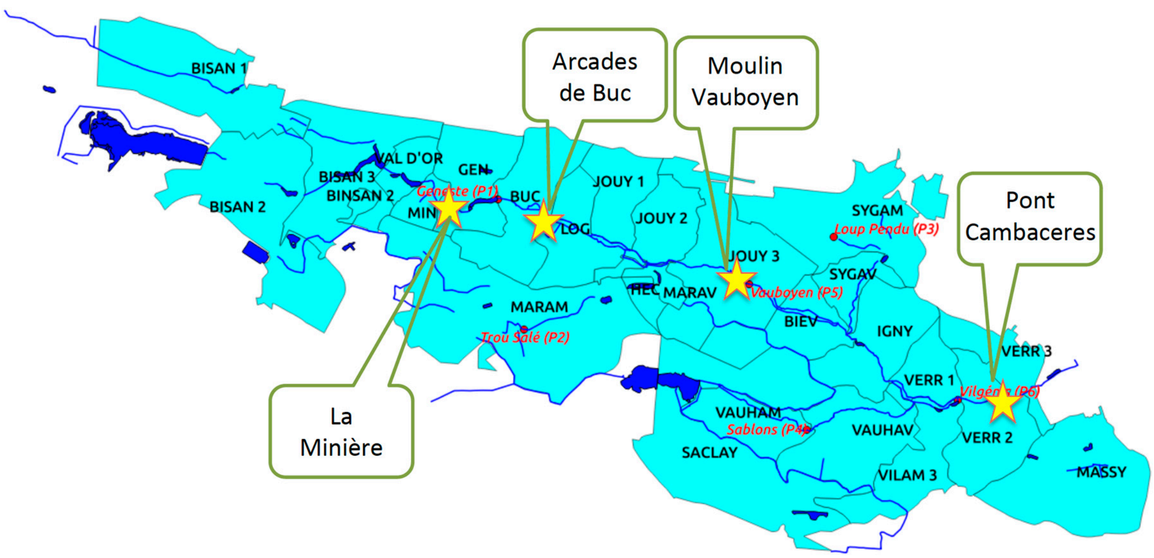

Figure 1. Illustration of the Bièvre catchment area with its representation in 27 sub-catchments used in InfoWorks CS. Five of them – BISAN1, BISAN2, BISAN3, BINSAN2 and VAL D'OR – belong to the CASQY-Bièvre catchment while the others belong to the SIAVB-Bièvre catchment. Location of six rain gauges over the SIAVB-Bièvre catchment and four measurement points are shown.

Preprints (www.preprints.org) | NOT PEER-REVIEWED | Posted: 14 October 2017 doi:10.20944/preprints201710.0096.v1

Following severe flood events in 1973 and 1982, local authorities started the construction of storage basins (integrated in the landscape) to limit the consequences of extreme events. 4 of these basins along the Bièvre River can be remotely regulated. In standard situation, basins are locally regulated according to downstream measured water levels, while on extreme situations an optimization of flows and storage capacity is done at the catchment scale using water levels in the river and in storage basins, along with rainfall data provided by six rain gauges (see Figure 1). The catchment scale regulation is automated although under a permanent human supervision.

2.2. Hydrological Model

The catchment is modeled with InfoWorks CS (Collection Systems), a widely used semi-distributed modeling software [40]. The area is divided into 27 sub-catchments, as displayed on Figure 1. Their sizes range from 0.3 to 11 km^2. The network as modeled is shown on Figure 2. This model is integrated in the Optim Sim platform, an off-line tool developed by Veolia that imitates the actual regulation of the storage basins either at the local or catchment scale. It is worthwhile to note that Optim Sim simulates in replays positions of gates that are not necessarily the same regulations that occurred during the real events. It should be also mentioned that the settings of neither InfoWorks CS model nor Optim Sim are fully up to date. For instance, a recent modification of the networks that consisted in the removal of the Vilgénis basin to restore the natural flow of the river (near "Vilgénis" rain gauge P6 on Figure 1) is not yet taken into account in the models. This difficulty pushes us in this study to focus on events without active regulation, i.e. when gates positions remain unchanged and therefore to focus on the differences associated with rainfall.

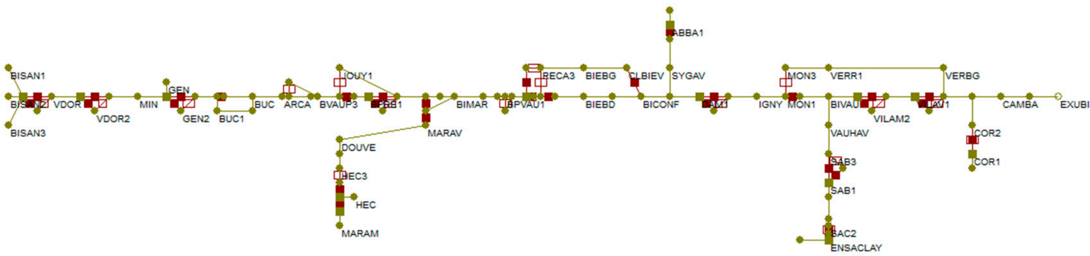

Figure 2. Bièvre InfoWorks CS model catchment.

There are two simulation modes in Optim Sim: the "replay mode" and the "forecasting mode". The first one enables to replay past events by extracting data from the linked database of the 6 rain gauges of the SIAVB. The rain rates for each sub-catchment are obtained using the Thiessen polygons technique. Then the simulations and observations (flood depth or flow at the measuring points) can be compared and analyzed. Since no other source rainfall data can be used with this mode, we have used the "forecasting mode". This second mode simulates the behavior of the river by introducing rainfall data from different possible sources, notably from (fully distributed) C-band radar measurements, although being converted in semi-distributed ones (i.e. a unique rainfall time series per catchment). It is also possible to use the forecasting mode for replays by merely setting past dates, thereby making it possible to compare the simulations with measured flow observations. Rainfall data can be input in three ways: an average intensity (mm/h) over all sub-catchments; a single average intensity time series over all sub-catchments; and an average intensity time series over each sub-catchment. In the last case, which we chose, a text file with a column containing rainfall intensity in mm/h with 5 min time steps has to be generated for each sub-catchment.

Practically, in order to generate the rain over each sub-catchment, we used the Bièvre catchment map with sub-catchment boundaries in GIS format along with the radar data ones (C-band and X-band). Then, we calculated the weighted average of the radar pixel rainfall rate values (R_{ij}) by the intersection area of the radar pixels (A_{ij}) with the sub-catchment areas $(A_{(sub-catchment)})$:

Preprints (www.preprints.org) | NOT PEER-REVIEWED | Posted: 14 October 2017 doi:10.20944/preprints201710.0096.v1

$$R_{(sub-catchment)} = \frac{\sum_{ij}\left[R_{ij}.\left(A_{ij} \cap A_{(sub-catchment)}\right)\right]}{\sum_{ij}\left(A_{ij} \cap A_{(sub-catchment)}\right)} \tag{1}$$

where the sum is made over all radar pixels (i, j).

In spite of the subdivision of the catchment for the InfoWorks CS model into 27 sub-catchments, as displayed on Figure 1 (and later on, Figure 9a), we used a version of the Optim Sim model with only 20 sub-catchments, i.e. homogeneous mean rainfall was introduced over the BISAN1, BISAN2, BISAN3, BINSAN2, VAL D'OR, GEN and MIN sub-catchments, as well as over SACLAY and VAUHAM, as illustrated by Figure 9b.

2.3. Three Selected Rainfall Events and Three Data Types

Three rainfall events that occurred in autumn 2015 were studied in this paper: 12-13 September 2015 (44 hours: 04:05 – 00:00), 16 September 2015 (16.8 hours: 00:05 – 16:50), and 5-6 October 2015 (31 hours: 09:10 – 16:05). These rainfall events last in total more than 90 hours, and were purposefully not split into many successive rainy periods as commonly done, which would have somehow artificially increased their number. Additionally, they were selected taking into account the hydrologic impacts on the Bièvre catchment as well as to cover the most common meteorological situations of the area. More precisely the rainfall of 12-13 September is due to two successive depressions coming from the British Islands (North-West) combined with the influence of Cevenol events from the South. The event of 16 September is associated with a storm Henry, generated by a former tropical depression coming from the South. It resulted in high winds. The 5-6 October event is associated with a depression coming from the West. A combination of stratiform and convective rainfall was observed during these events. It means that these events are altogether sufficiently representative for the purpose of this study. The first two events triggered an optimization of the river management at the catchment scale, while only local regulations (with no optimization at all) were used for the third one.

Over the Bièvre catchment (see Figure 3), the rainfall data could be provided from three different sources:

- The SIAVB network of six tipping bucket rain gauges, being distributed over the catchment;
- The Météo-France polarimetric C-band radar of Trappes, being located in a direct proximity (~ 0 - 20 km) of the catchment;
- The ENPC polarimetric X-band radar of Champs-sur-Marne, with distances ranging between 25 to 45 km;

Preprints (www.preprints.org) | NOT PEER-REVIEWED | Posted: 14 October 2017 doi:10.20944/preprints201710.0096.v1

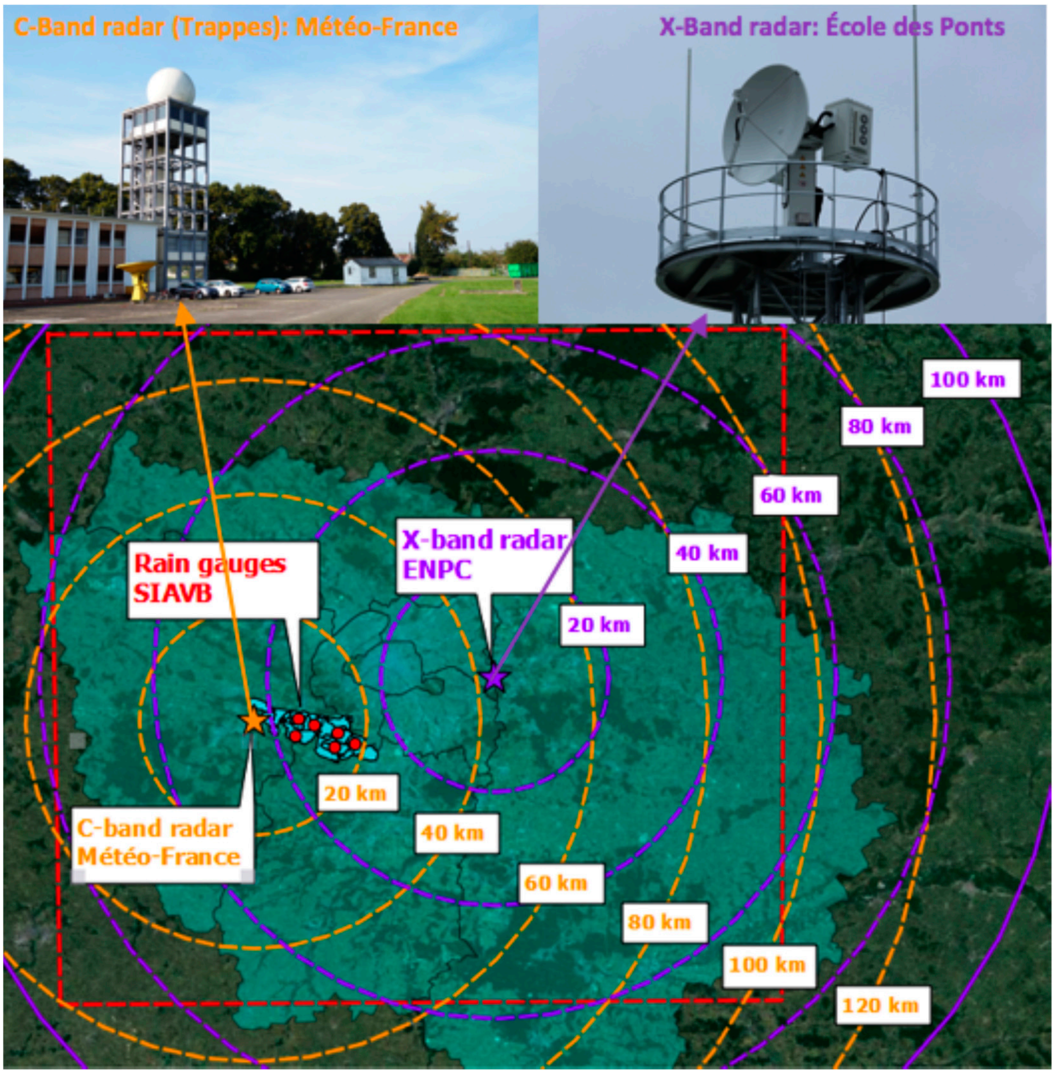

198 **Figure 3.** Illustration of rainfall measurement devices available over the Bièvre catchment. The square
199 area (red dashed line) is the 128 x 128 km² area, covered by the two radars.

200 *2.4. Radar Data Processing*

201 2.4.1. From Météo-France

202 For its C-band radar products, Météo-France uses standard Z-R relation [41] to convert corrected
203 reflectivity factor ($Z\ (mm^6.m^{-3})$) to rain rate $R(mm.h^{-1})$:

$$Z = aR^b \quad (2)$$

204 with parameter values being fixed as a=200 and b=1.6.
205 The data provided by Météo-France is the radar mosaic for precipitation amount over the whole
206 territory generated with the help of its radar network, initially called Aramis [42]. Within the
207 PANTHER project (Aramis New Technologies Hydrometeorology Extension and Renewal), this
208 network includes 29 radars. Being spread over the entire territory, the radars have a range of about
209 100 km to measure the amount of precipitation and about 200 km to detect them. A number of
210 "individual radar" products are transmitted every 5 minutes to the Météo-France center in Toulouse.
211 Mosaics are then constructed from these products by selecting for each pixel the individual radar
212 information with best quality. Given that the Bièvre catchment is located very close to the
213 polarimetric C-band radar of Trappes (~ 25 km maximum), the mosaic data come only from the
214 Trappes radar.

Preprints (www.preprints.org) | NOT PEER-REVIEWED | Posted: 14 October 2017 doi:10.20944/preprints201710.0096.v1

In the PANTHER products, the incremental rainfall accumulation is calculated at time steps of 5 minutes. It results from many post-treatments that manage the common radar issues of partial masks, bright band, fixed echoes and signal attenuation. For example, Gourley et al. [43] suggested that the specific attenuation is related to the specific differential phase with the help of a simple linear relation and calibrated it for the Trappes radar. Since February 2012, the double polarization is used, but exclusively for the attenuation and clear air corrections, it does not take into account the biases introduced by large scale drops and therefore the different rainfall regimes. The ratio of reflectivity and incremental accumulation therefore requires calibration in real time, which is evenly performed over the entire area of the radar (radius of about 100 km) and according to a quality code based on the last twelve hours rain gauge radar comparison. This ratio is calculated in particular for correcting a slow drift of the measurement and is used to trigger the appropriate intervention for radar maintenance.

2.4.2. From ENPC

The ENPC X-band radar rainfall data were processed with the standard Rainbow software [44]. Due to the initial choice of the pulse width and angle step, the highest resolution of pixel in the radial direction is 250 m only and 3.4 min in time. Hence, a more appropriate choice of scan/scheduler parameters could further improve the space-time resolution of the rainfall products for the Bièvre catchment.

In this study we use the Dual Polarization Surface Rainfall Intensity (DPSRI) product. Contrary to the Surface Rainfall Intensity (SRI) product, it is not generated only with the help of the horizontal reflectivity data, but also uses the vertical one with the help of the differential reflectivity, ZDR, and the specific differential phase, KDP. The signal of the differential phase shift is quite noisy and, in practice, it is smoothed before computing the specific differential phase. The Rainbow software proposes a choice of several sophisticated smoothing methods, starting from the classical filter that is based on a (weighted or non-weighted) moving average, a median filter (which produces the simply filtered KDP) up to the Finite Impulse Response (FIR) filter. The resulting specific differential phase is almost independent of attenuation and partial beam blocking by attenuation. Figure 4 illustrates an example of estimated rainfall (in dB scale), resulting from FIR filtered signal. This figure can be compared with the Figure 5, exhibiting the same quantities with simply filtered KDP.

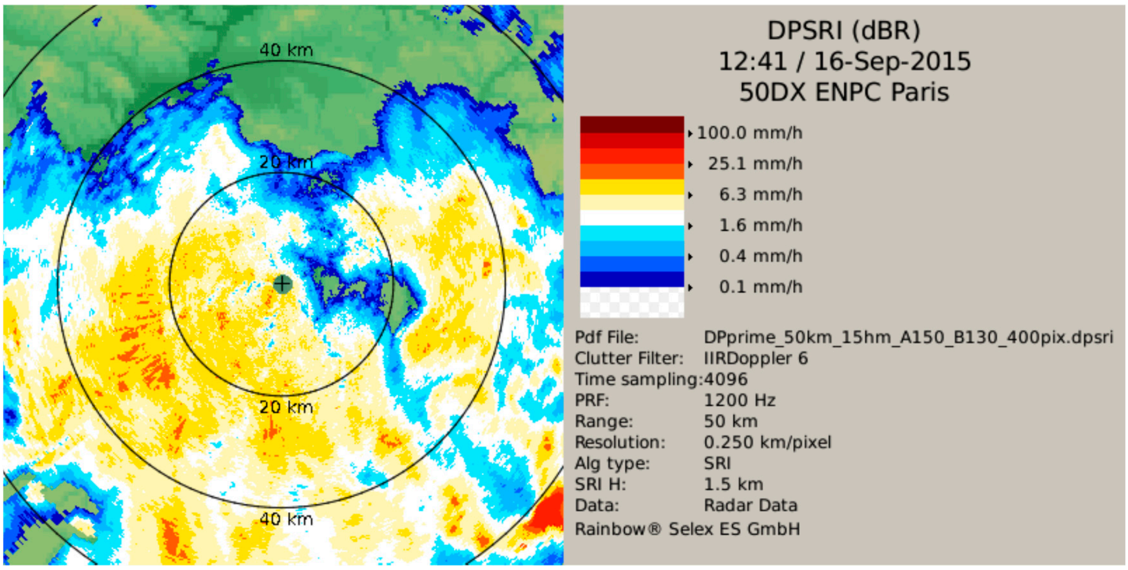

Figure 4. Icon of the standard Rainbow software (Selex copyright): DPSRI product of rainfall intensity (in dB scale) using FIR filter.

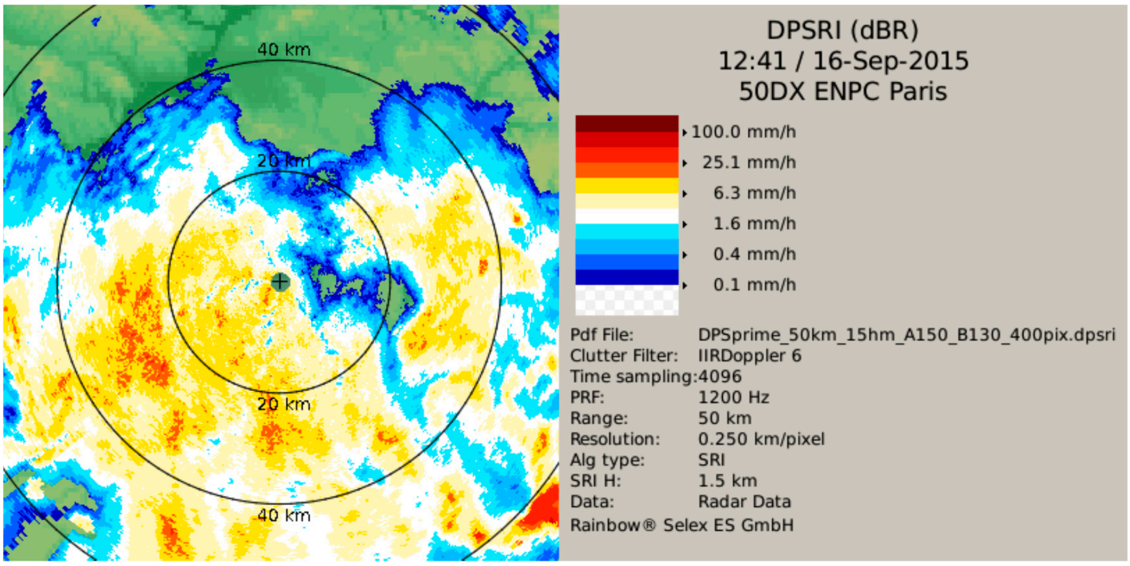

Figure 5. Icon of the standard Rainbow software (Selex copyright): DPSRI product of rainfall intensity (in dB scale) using simple filter.

The DPSRI Selex product uses a hybrid radar algorithm with a Z-R relation used at only for very low intensities and R-KDP for higher intensities:

$$R = 19.63|KDP|^{0.823}, \qquad \text{for Z} > 35\ dBZ\ and\ KDP > 0.3\ deg/km \tag{3a}$$

$$Z = aR^{b} \qquad , \qquad \text{else} \tag{3b}$$

To illustrate the influence of the choice of either Selex data filtering procedures or parameters for the DPSRI at 1.5 km, the time evolution of ENPC X-band radar rainfall accumulations over the six sub-catchments containing the rain gauges is considered here, for the event of 12-13 September 2015. Firstly we use the FIR filtered KDP with the Z-R parameters a=200 and b=1.6, those applied by Météo-France for the C-band radar in Trappes. Then, we change the Z-R parameters to a=150 and b=1.3, using either FIR or simply filtered KDP. Figure 6 displays the obtained results that suggest two intermediate conclusions. By comparing the left and middle graphs, the first observation is that, in spite of the fact that the change of Z-R parameters for DPSRI modifies only very low rainfall intensities (lower than typically 7 mm.h^{-1}), this change increases the rainfall totals by about 40%. This simple analysis highlights how critical the choice of a and b parameters is, furthermore considering the wide range of possible values discussed in the literature [examples among others: 41,45,46]. By comparing the middle and right graphs, the second observation is that simply filtered KDP results in a slight increase in the rainfall estimates. A similar behavior was observed for two other events. Selecting the appropriate radar algorithms remains a challenging, methodological, observational question that has far-reaching implications on water management. In the next section we innovatively use Multifractal Analysis to help to choose which X-band radar product will be used for the hydrological modeling. To the knowledge of authors, this is the first time that such methodology is developed.

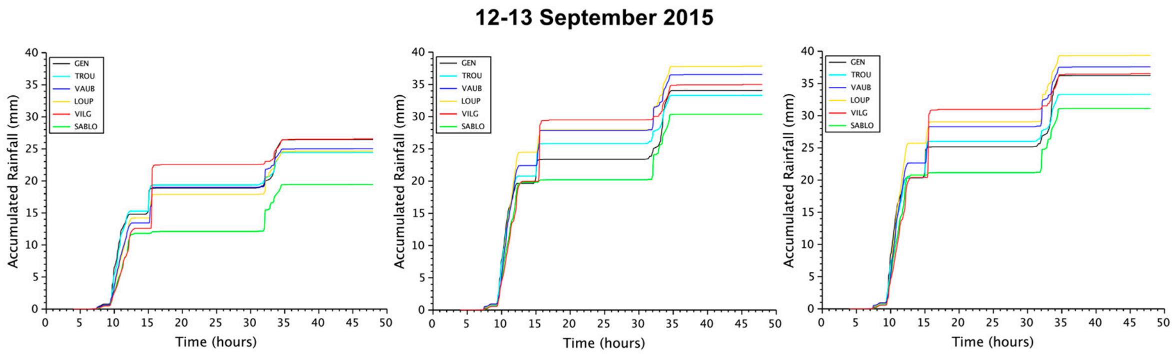

Figure 6. Time evolution of accumulated X-band rainfall during the event of 12-13 September 2015 over six catchments containing the rain gauge: GEN (P1 Geneste/GEN), MARAM (P2 Trou Salé/TROU), SYGAM (P3 Loup Pendu/LOUP), VAUHAM (P4 Sablons/SABLO), JOUY3 (P5 Vauboyen/VAUB) and VERR2 (P6 Vilgénis/VILG). The three DPSRI rainfall products at 1.5 km were obtained with: FIR filter and Z-R parameters a=200 and b=1.6 (left); FIR filter and Z-R parameters a=150 and b=1.3 (centre); and simple filter and Z-R parameters a=150 and b=1.3 (right).

3. Results

In this section, we study the space-time rainfall variability detected by the radars of both types. The multifractal framework is particularly appropriate for analysis of such highly intermittent fields and is expected to better differentiate the rainfall products. Indeed, it enables a comparison across scales and not only at a given scale as classically done. This yields more robust conclusions, notably when the observation scales of the two measuring devices are not the same as it is the case here. Then we discuss the results of hydrological comparison performed with the best rainfall products available for each of the radars. The present results have most presumably significant implications on the rainfall physics that would need to be further explored elsewhere.

3.1. Direct Comparison of Rainfall

3.1.1. Short Recap on Multifractals

Multifractals have been developed and applied to analyze and simulate geophysical fields exhibiting extreme variability over a wide range of scales such as rainfall [29,47–65]. For such fields the statistical moment of order q of a field R at the resolution λ ($= L/l$, where L is the outer scale of the phenomenon and l the observation scale) is a power-law behavior related to the resolution:

$$\langle {R_\lambda}^q \rangle \approx \lambda^{K(q)} \tag{4}$$

where $K(q)$ is the statistical moment scaling function that fully characterizes the scaling variability of the studied process.

The trace moment (TM) analysis, which consists in checking the validity of equation 4, enables to confirm the scaling behavior of the field. More precisely moments for various resolution are computed by up-scaling the field from its maximum resolution, then equation 4 is plotted in a log-log scale for various q, and straight lines of slope $K(q)$ are retrieved for multifractal fields. In this paper, we study 2D rainfall fields. The rainfall maps for each time step are upscaled independently and the average of equation 4 computed then over the ensemble of time steps.

Figure 7 displays the TM curves obtained over the full duration of the 12 September 2015 rainfall event for three Dual Polarization Surface Rainfall Intensity (DPSRI) X-band radar rainfall products at 1.5 km and C-band radar data. Maps of the size 64 km x 64 km are analyzed up to the resolution $\lambda = 1$. In all cases a single scaling behavior is considered. Figure 7a displays the result of trace moment analysis for the FIR filtered DPSRI product with Z-R parameters a=200 and b=1.6. One may note that there is a strong curvature of the TM curves, and hence this product is not really in agreement with the expected and widely reported in the literature scaling behavior of the rainfall fields. The

Preprints (www.preprints.org) | NOT PEER-REVIEWED | Posted: 14 October 2017 doi:10.20944/preprints201710.0096.v1

multifractal scaling behavior of the DPSRI products with Z-R parameters *a*=150 and *b*=1.3 is much more evident (Figures 7b and 7c, for FIR and simple filter, respectively). It confirms that this change of parameters improves the scaling, while it increases the rainfall intensity maxima. Based on these analyses and on the fact that the choice between FIR and simple filter does not make a significant difference, the X-band product chosen to be used hereafter was the DPSRI with FIR filter, and *a*=150 and *b*=1.3 for low intensities. Refining this analysis using this methodology is outside the scope of this paper and will be done in future studies. Finally, Figure 7d displays the TM analysis result for the C-band radar data. This figure shows that it also has a great scaling behavior, not to mention the fact that there are less points than the X-band ones because of the small scale spatial resolution difference (250 m for X-band, and 1 km for C-band).

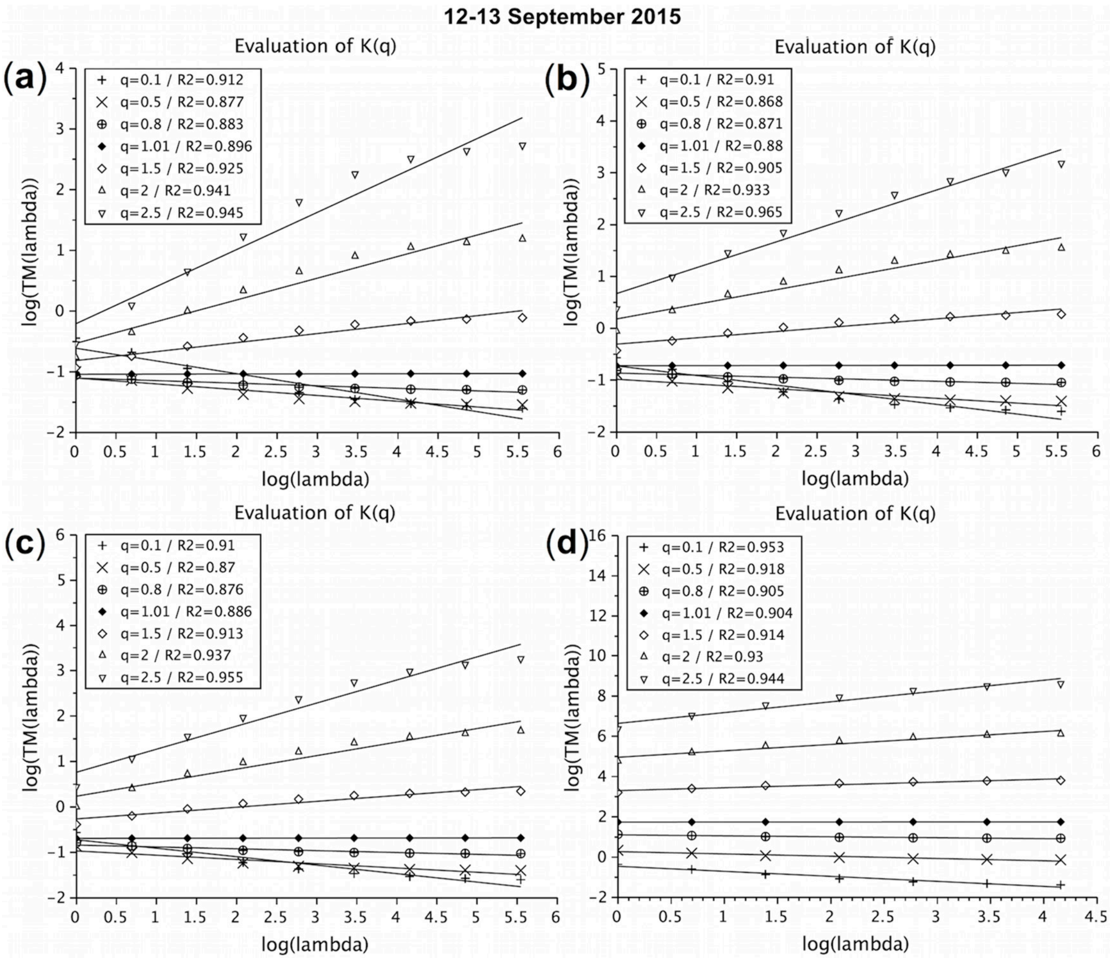

Figure 7. TM (equation 4 in log-log plot) analysis for the 12-13 September 2015 event: X-band DPSRI rainfall products at 1.5 km obtained with a) FIR filter and Z-R parameters a=200 and b=1.6 for low intensities, b) FIR filter and Z-R parameters a=150 and b=1.3 for low intensities, c) simple filter and Z-R parameters a=150 and b=1.3 for low intensities; and d) C-band rainfall fields.

It is important to note that for the X-band DPSRI products, a change of scaling regime may also occur for scales smaller than 1 km, but given the limited number of points, it is not possible either to confirm or infirm this consideration. Should the break indeed be real, it would mean that rainfall structures and extremes could not be extrapolated from measurements at larger scales. The overall estimates of the coefficient of determination R^2, being used as a metrics of scaling behavior, are lower for X-band radar data. A somewhat similar scaling behavior is found for the other two rainfall events.

A specific multifractal framework is that of Universal Multifractals (UM), toward which multifractal processes converge under rather wide conditions [47,66,67]. Conservative multifractal fields, whose mean is strictly conserved through scales, are characterized with the help of only two parameters: C_1>0, the mean intermittency co-dimension, measuring the mean intermittency, that of the average intensity ($C_1 = 0$ for a homogeneous field) and $\alpha \in [0,2]$, the multifractality index which measures the variability of the intermittency with statistic orders. In this case, the statistical moment scaling function $K(q)$ is then given by:

$$K(q) = \frac{C_1}{\alpha - 1}(q^{\alpha} - \mathrm{q}) \quad (5)$$

We assessed the UM parameters of the three selected events by using the Double Trace Moment (DTM) technique [68], for both C-band and X-band (DPSRI; FIR filter; a=150 and b=1.3 for low intensities) radar data. Table 1 summarizes the UM parameter estimates. It is important to note that the estimates summarized in the table are computed over the full range of considered space scales, i.e., 1-64 km for the C-band radar and 0.25-64 km for the X-band radar. At the same time, it will be fruitful to mention that the overall estimates of R^2, being used as a metrics of the scaling behavior, are lower for the X-band radar data, mainly because changes in scaling may occur over smaller scales that are not available with the C-band measurements. We tested that two scaling regimes with distinct linear fits in a log-log plot yield two distinct pairs of UM parameters for the X-band spatial rainfall. While the multifractality parameter estimated over large scales (1-64 km) becomes closer to that obtained for the C-band radar data (on the same range), the DTM estimator gives spurious multifractality parameter (>2) over the small scales (0.25-1 km, unknown for the C-band radar). This could be due to the emergent properties of rainfall extremes at small scales. Indeed, a well-known basic property of precipitation is that small-scale extremes (short duration or/and size, e.g. heavy rainfall episodes) can drastically influence much larger scales (e.g., yearly statistics and even climate) to the point of creating heavy tails for the probability of larger scale extremes. This basic feature remains out of reach from (quasi-) linear models (e.g. the still used Scott-Newman model and variants), whereas it is generic in multifractal cascade models.

Table 1. UM parameters of the three events.

Event	Radar	Start time	Duration (hours)	Time steps	α	C_1
12-13 Sept 2015	C-band	04:05	44	528 (5 min)	1.25	0.22
12-13 Sept 2015	X-band	04:05	44	773 (3.4 min)	1.54	0.18
16 Sept 2015	C-band	00:05	16.8	202 (5 min)	1.02	0.12
16 Sept 2015	X-band	00:05	16.8	296 (3.4 min)	1.51	0.11
5-6 Oct 2015	C-band	09:10	31	372 (5 min)	1.58	0.15
5-6 Oct 2015	X-band	09:10	31	545 (3.4 min)	1.79	0.15

In Table 1, one can verify that, for each of three rainfall events, the α parameters are greater for the X-band radar data than for the corresponding C-band ones, though the C_1 parameters remain almost the same for both radar data types. These results mean that the X-band radar data have stronger extremes (having more "peaks"), while a similar intermittency of the average intensity. This result needs to be confirmed on a wider sample, but already emphasizes the importance of having high-resolution precipitation data not to miss the very local rainfall extremes. It is important to note that such more pronounced variability found on X-band data does not necessary imply that the X-band rainfall rates are higher than the C-band ones.

Preprints (www.preprints.org) | NOT PEER-REVIEWED | Posted: 14 October 2017 doi:10.20944/preprints201710.0096.v1

3.1.2. Rainfall Estimates over the Catchment

This subsection intends to give an overview of the rainfall data resulting from different measuring techniques (SIAVB rain gauges, X-band and C-band radar data) for each of three events: 12-13 September 2015, 16 September 2015 and 5-6 October 2015 over the whole catchment area. Whereas all measuring techniques overall agree on the dynamics of the total rainfall during the studied events, there are some significant differences among the rainfall estimates. It seems that they are primarily occurring during low rainfall periods for which the choice of parameters in the Marshall-Palmer relation is crucial as previously discussed.

Figure 8 displays maps of the total cumulative rainfall depth, for X-band and C-band rainfall measurements along with the SIAVB rain gauges estimates (circle) for the studied rainfall events. Rain gauge data was not available for the last event. The color pallets remain the same for all data types for each event. It appears that C-band data yield greater estimates than those of the X-band.

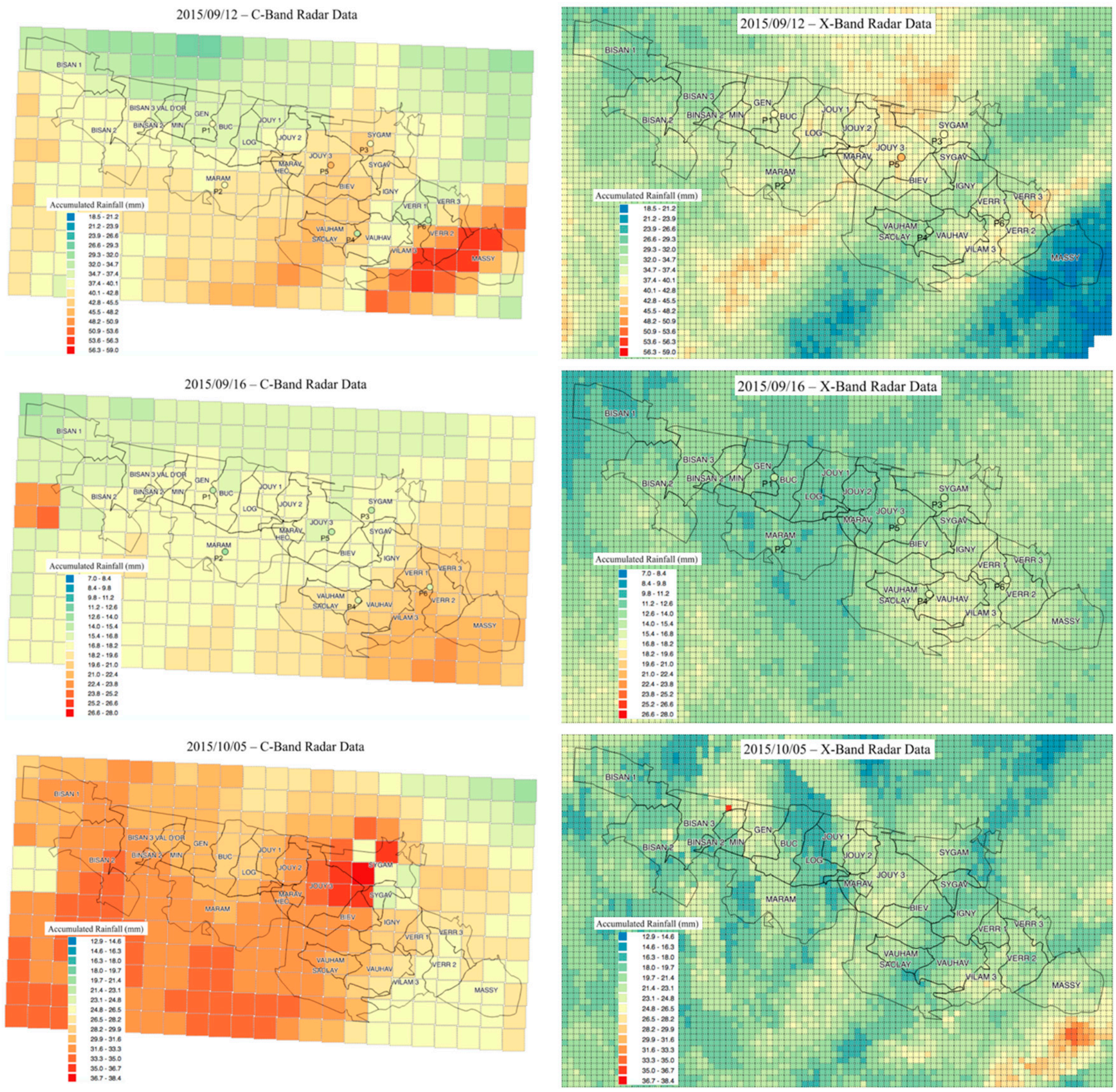

Figure 8. C-band (left) and X-band (right) pixel maps of the rainfall totals, using the same color pallets, for the three events studied: 12-13 September 2015 (top), 16 September 2015 (center) and 5-6 October 2015 (bottom). Six circles indicate the rain-gauged values, just for the first two events.

Additionally, Figure 9 displays maps of the C-band, X-band and rain gauged rainfall totals per each sub-catchment (calculated by using equation 1, as discussed in Section 2.2) and six circles correspond to the SIAVB rain gauges for the 12-13 September 2015 event. Such five-minute totals per sub-catchment actually correspond to the rainfall data input into the hydrological model. Figures 8

Preprints (www.preprints.org) | NOT PEER-REVIEWED | Posted: 14 October 2017 doi:10.20944/preprints201710.0096.v1

and 9 illustrate well the loss of information with regards to rainfall when considering only a limited number of sub-catchments. Comparing the C-band and X-band rainfall totals to those resulting from the SIAVB tipping bucket rain gauges, one may note that the X-band radar tends to underestimate, while C-band radar mostly overestimates them. However, these observations remain non-conclusive due to the fact that the rainfall is strongly variable at small scales, and totals measured by a single rain gauge are not necessary representative at the scale of whole catchment. However, for the two other events (not illustrated in this paper), the X-band rainfall accumulations are also lower than the C-band ones.

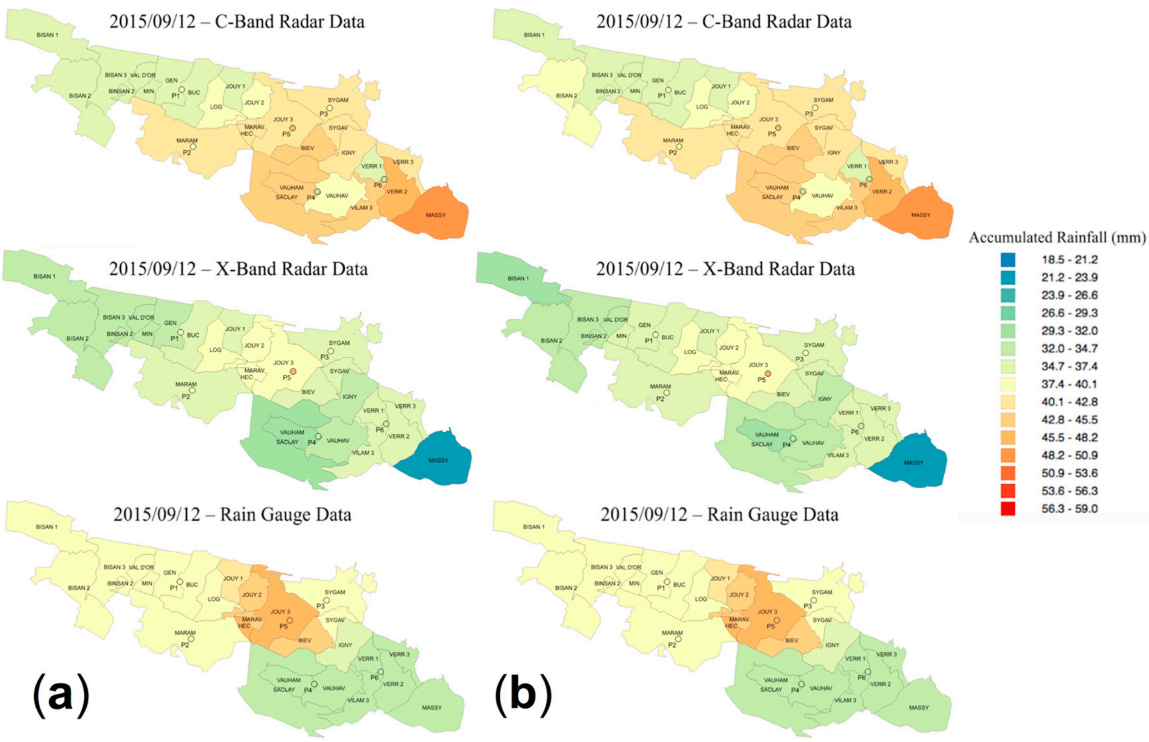

Figure 9. Maps of the C-band (top), X-band (center) and rain gauged (bottom) rainfall totals per each of a) 27 sub-catchments and b) 20 sub-catchments. Six colored circles indicate the corresponding rain gauged values.

Finally, Figure 10 compares the time evolution of the accumulated rainfall (C-band and X-band radars), either per catchment containing the SIAVB rain gauges or by the corresponding pixels during the 12-13 September 2015 event for illustration. This time, the differences between the rainfall totals estimated per pixel or per sub-catchment for the same radar type highlight the misrepresentation of a single point as the whole catchment, as discussed earlier. In two locations the X-band radar gives estimates closer to the rain gauge estimates (SYGAM and VAUHAM), while in two others (MARAM and JOUY3) the C-band radar does. In the two remaining locations (GEN and VERR2) their differences remain comparable. Except for the C-band in VAUHAM, these differences remain inferior to the uncertainties induced by the unmeasured (below the radar observation scale) rainfall variability [12]; making it difficult to compare directly the rainfall estimates. This illustrates well the contribution of the multifractal analysis carried out in this paper, which proposes a comparison framework independent of an observation scale, as well as the need for further hydrological modeling that would reduce the uncertainties of multifractal parameters estimation.

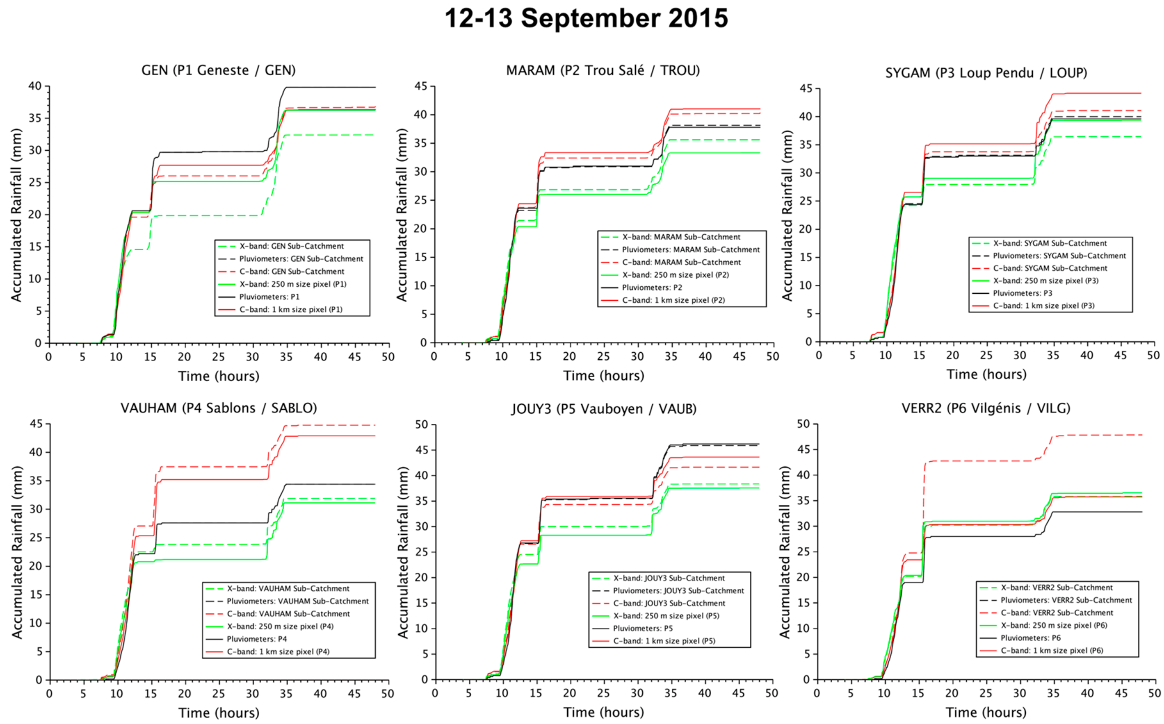

Figure 10. Comparison of accumulated rainfall per catchment (dashes) and per rain gauge pixel (solid line) during the event of 12-13 September 2015 for rain gauge (black), C-band (red) and X-band dual pol (green; FIR filter; a=150 and b=1.3 for small intensities) rainfall data.

3.2. Hydrological Comparison

As already indicated, the goal of this study is a hydrological comparison of the rainfall data resulting from C-band and X-band radar measurements notably to study the impact of small-scale rainfall variability over the Bièvre catchment. We use in this work the Optim Sim model (coupled with InfoWorks CS) as described in Section 2.2.

Simulated flows are compared with observations at four locations from upstream to downstream (see Figure 1): "La Minière", "Arcade de Buc"; "Moulin Vauboyen" and "Pont Cambaceres". "La Minière" is actually the point where the portion of the Bièvre River managed by the SIAVB starts, while the upstream area is modeled to simulate the flow entering the SIAVB territory. "Pont Cambaceres" is the only point located downstream the Vilgénis basin (not existing anymore, but still remaining in the model). However, this situation could have only limited impact on simulation outputs because the unregulated flow should remain rather similar whether the basin is removed or not.

These four locations correspond to an increasing number of regulated storage basins: none for "La Minière", while two for "Arcades de Buc", three for "Moulin Vauboyen" and seven for "Pont Cambaceres". This implies that the simulated outputs downstream will potentially be more affected by a regulation at the whole catchment scale, i.e., at "Pont de Cambaceres" than at "La Minière".

Figure 11 displays the flow simulated at "Arcades de Buc" with X-band data for the 16 September event. The simulations are carried out either with or without the implementation of the tool mimicking regulation at the catchment scale. While all simulations presented below perform at a 5 min time step, the time step of update of gate positions remains of 15 min. It is possible to reduce it to 5 min as well, but it would multiply by three the computation time. Although it could affect the results, it is likely that it does not really in this case because the model's sensitivity to the time step is rather low due to the size of the sub-catchments. As it can be seen from this figure, the observations are situated right in between the two simulations using the X-band radar data, with and without the implementation of the Optim Sim tool. The differences are very significant, showing that the regulation has strong consequences. It illustrates well the difficulty to actually compare simulations with observations given the previously mentioned limitations of this tool. Nevertheless, for the 5-6

Preprints (www.preprints.org) | NOT PEER-REVIEWED | Posted: 14 October 2017 doi:10.20944/preprints201710.0096.v1

October event, optimization of the regulations at the catchment scale was actually implemented only at the end of the simulated period, meaning the comparison with observations is more relevant and more convincing in the first part of the event.

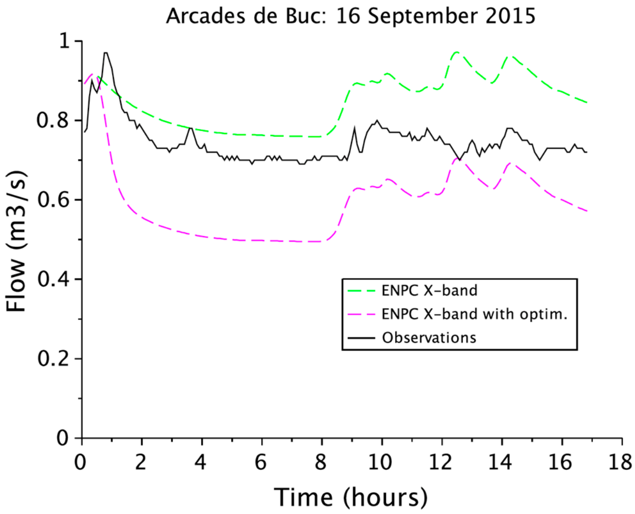

Figure 11. Flow simulated at "Arcades de Buc" with X-band data for the 16 September event. Simulations are carried out with or without the implementation of the tool mimicking regulation at the catchment scale.

Figures 12-14 display the simulated flows at the four selected points for respectively the 12-13 September event, the 16 September event and the 5-6 October event. The tool simulating the regulation at the basin scale was not used. All C-band data, X-band data and SIAVB rain gauge network were tested and inter-compared.

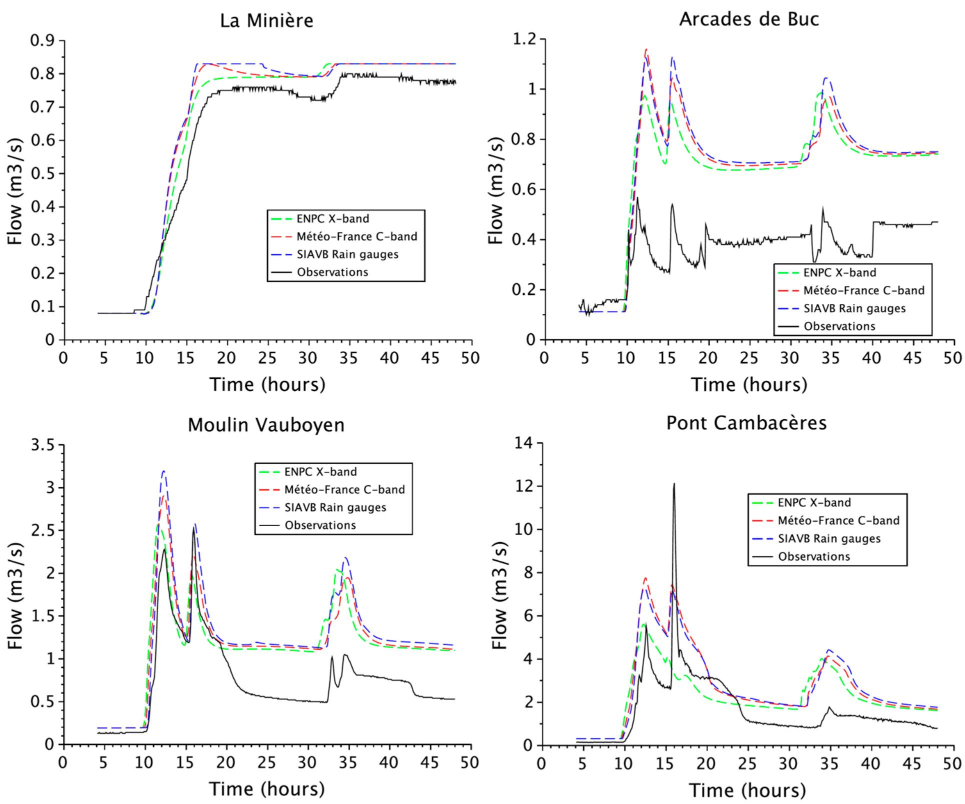

Figure 12. Flow simulated at the four studied locations with X-band data for the 12-13 September event, along with observations. Simulations are carried out without the implementation of the tool mimicking regulation at the basin scale.

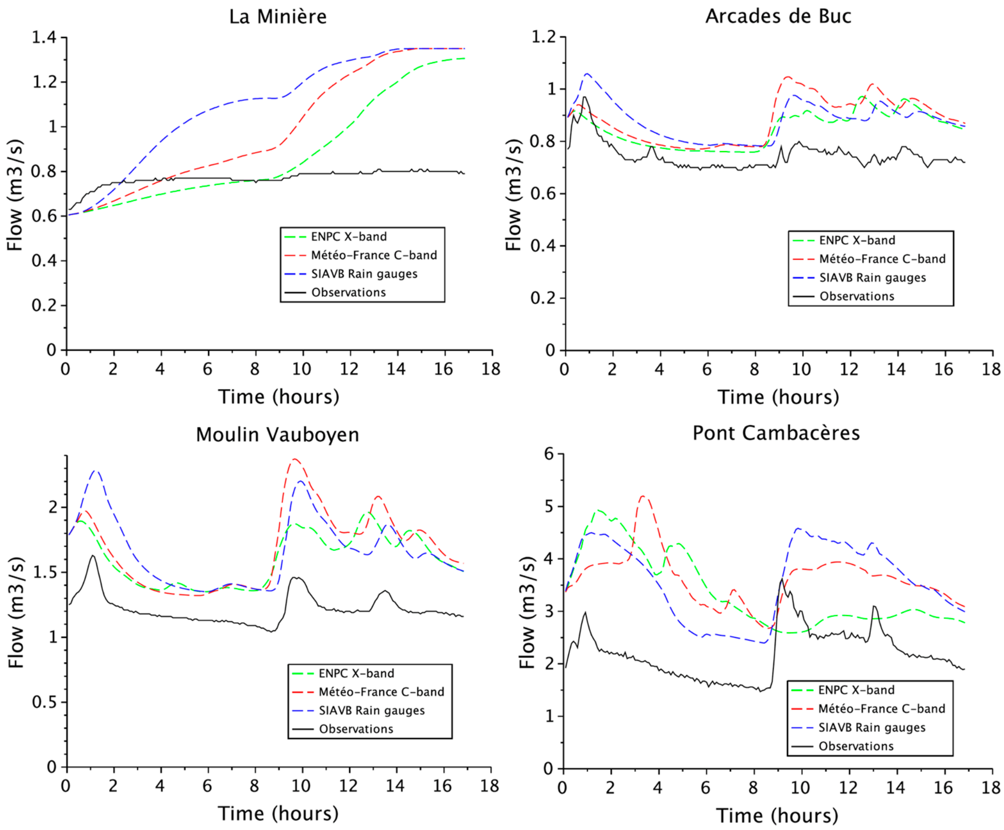

Figure 13. Flow simulated at the four studied locations with X-band data for the 16 September event, along with observations. Simulations are carried out without the implementation of the tool mimicking regulation at the basin scale.

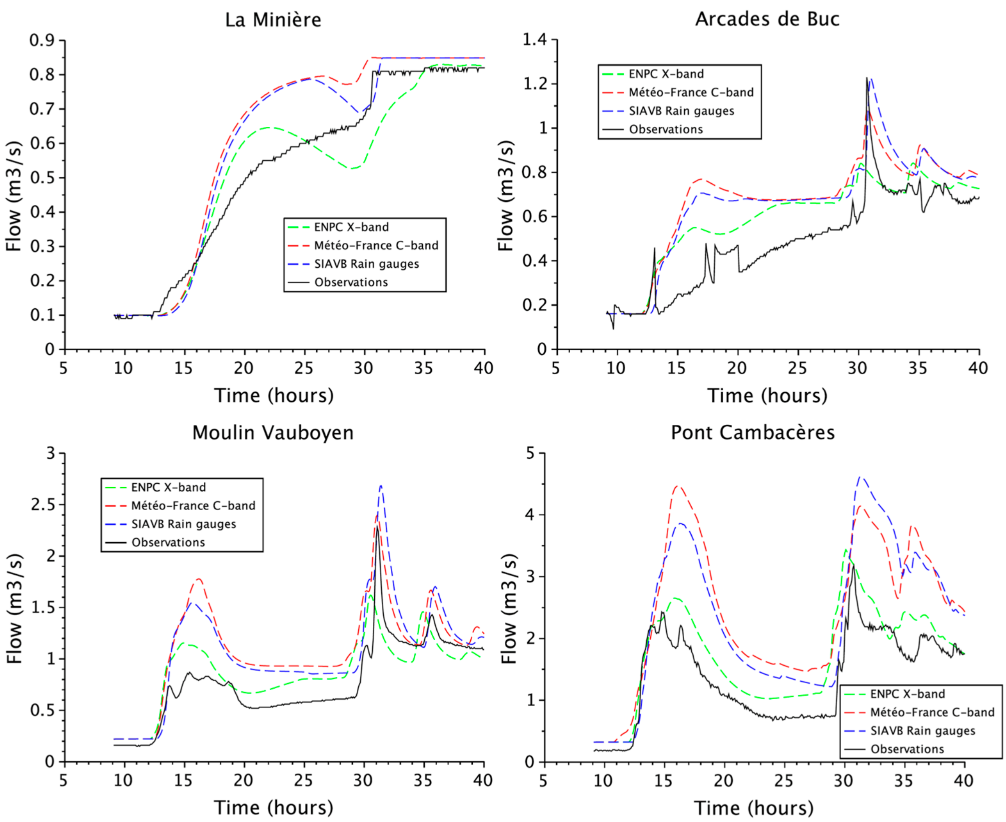

Figure 14. Flow simulated at the four studied locations with X-band data for the 5-6 October event, along with observations. Simulations are carried out without the implementation of the tool mimicking regulation at the basin scale.

For the 12-13 September event (Figure 12), the increase of flow at "La Minière" location reaches its regulated target value of 0.8 m^3/s, being well reproduced with the three rainfall products. The fact that regulation at the catchment scale is not mimicked makes comparison with observations not relevant, as discussed above. For this event there is a tendency of the X-band data to generate slightly smaller flows than the other two products, well visible on all curves of the figure. This tendency is more pronounced for the first half of the event (until 13 September 2015 at 07:00) than for the second one. A small time shift is visible with the X-band data for the third peak (13 September 2015, ~ 11:00). This artifact is due to a simplification carried out in the conversion of the rainfall data from the initial temporal resolution of 3 min 25 sec to the required one of 5 min for Optim Sim.

For the 16 September event (Figure 13) the simulated flows are much greater than observed ones, for which the optimization of the outflow regulations of the catchment was deployed, again highlighting the issue with the simulation of local regulation for this event. It is important to mention here that the values observed at "La Minière" are greater than the 0.8 m^3/s regulated target value because additional water coming from an overflow at Val d'Or is input in the model for this event. This should be investigated more precisely in future work. The differences between the three rainfall products on the simulated flows are more pronounced for this event than for the other two. It should also be noted that there are some changes according to the observation point and time. For instance, at the beginning of the event (before 16 September 2015 at ~ 05:00), rain gauges yield a greater flow at "Arcades de Buc" and "Moulin Vauboyen" whereas it is at "Pont Cambaceres" for the X-band radar. At this location the C-band rainfall data generate a peak that is found neither with other rainfall data nor on observations. In the period between 08:00 and 16:50 on 16 September 2015, C-band data yield greater flows at "Arcades de Buc" and "Moulin Vauboyen" (more pronounced for the beginning of this period) whereas it is the rain gauges at "Pont Cambaceres". Here the simulated flows are much smaller with X-band data. As for the 12-13 September event, it is not relevant to compare with actual measurements due to the problematic simulation of regulation at the catchment scale that was actually deployed.

As previously mentioned, for the 5-6 October event, the regulation at the basin scale was only enforced at the end of the event, meaning that comparison with observations is more relevant (see Figure 14). At "Arcades de Buc", there is overall less overestimation of flows, but it should be noted that the peak at about 12:00 on 6 October 2015 is underestimated with the X-band radar data. Similar patterns are found at "Moulin Vauboyen" with a lower underestimation for the peak. At "Pont Cambaceres", simulations with X-band data reproduce well observations whereas there is an overestimation with C-band data and rain gauges. It is interesting to note that despite the rather higher level of processing – calibration (performed for many years) and real time adjustment in real time to rain gauges – of the C-band radar is not so successful with respect to the (unadjusted, uncalibrated) dual-polarimetric data of the X-band radar. This finding is all the more interesting given that, as pointed out before, the C-band radar has the advantage to be closer to the test site than the X-band radar (20 km vs. 40 km) putting it a better position from the beginning.

It turned out that comparison with distributed data in replay mode was more difficult than expected due to the necessary update for the tool mimicking actual real time control of the river network. In general, for the first two events, the X-band radar data yields slightly lower simulated flows. It is also the case for the last rainfall event, where observations tend to validate the use of X-band radar data, although there are some discrepancies on a peak.

4. Discussion

First, it is worthwhile to recall in which conditions the present results were obtained:

- The Bièvre test site is about 40 km far from the ENPC X-band radar, whereas it is only about 20 km from the Météo-France C-band radar;
- The Bièvre catchment has a very complex topography, e.g. with very steep slopes, that has various influences on the rainfall (micro orographic effects), its detection (ground clutter) and the runoff;

- The ENPC X-band radar had only a one point calibration, i.e. to test the equivalence of the vertical and horizontal reflectivity's for an isotropic scattering (such as the solar radiation that is used for this test), but no absolute calibration was used up to now;
- No calibration was done for the Z-R relation parameters, whereas this relation was used for low reflectivity's;
- Furthermore, no adaptation to either rain gauges or rainfall tracking was performed;
- In the future, the Selex hydrological products eventually could be calibrated with the help of site available disdrometers;
- The scan strategy was chosen for a volumetric exploration of the 3D-nature of the rainfall, more precisely only 2 scans over ten have an elevation below 2.5°;
- Furthermore, the rotation rate was kept uniform (24°/s) for all elevations;
- The ENPC X-band radar rain rate estimates were obtained by the product DPSRI (Double Polarization Surface Rainfall Intensity) at 1.5 km height over the ground, whereas the C-band estimates corresponds to the data having the highest quality indicator over the pixel vertical;
- The InfoWorks CS model configuration having only 20 sub-catchments washes out the observable variability among the sub-catchments of the CASQY-Bièvre catchment and two sub-catchments of the SIAVB-Bièvre catchment, clearly impacting the results of hydrological modeling.

It is therefore interesting to note that in such conditions a semi-quantitative agreement was obtained by the X-band radar estimates with respect to the in-situ observations and those of the Météo-France C-band radar (with a higher level of processing: calibration performed for many years and real time adjustment to rain gauges). Two differences are also worthwhile to note and to discuss: as expected, the X-band radar was able to pick up a few extremes that were smoothed out by the C-band radar; on the contrary, the DPSRI product of the X-band radar seems to have underestimated low intensity episodes of the chosen events. The latter might be explained by both the chosen data processing and acquisition strategies. However, this requires to be further investigated, as discussed below.

This study should be therefore considered as a very first attempt to compare the X-band and C-band radar rainfall products using hydrological models. As already mentioned, further investigations are required. They are of two types:

- Those that can be achieved with the past data, i.e. without changing the data acquisition: they correspond to modify given stages of the data processing chain leading to a given type of rainfall estimate. Main options include: at least two different methodologies to estimate the specific differential phase shift (KDP), using differently the double polarization (e.g. the KDP-R relation including for low reflectivity's), attenuation correction, different heights for the product DPSRI, defining other products (e.g. closer to those used by Météo-France);
- Those that cannot be achieved with the past data, i.e. changing the data acquisition. This includes modifying: the scan strategy, the pulse repetition frequency and the pulse length itself.

Both lists show a large choice of possible settings for respectively data processing or data acquisition. The former was slightly investigated, although not presented in this work. Further X-band radar tests and comparative studies are necessary in order to ensure the optimal measurement capability.

A last, but not least, remark corresponds to the necessity to proceed to similar studies on other test sites, in particular those being located at a similar distance from both radars.

Supplementary Materials: Data can be accessed at http://doi.org/10.5281/zenodo.840992.

Acknowledgments: The authors greatly acknowledge partial financial supports of the Chair "Hydrology for resilient cities" endowed by Veolia, and of the Department of Science and Technology of the Brazilian Army. The authors are thankful to M Bernard Urban (Météo-France) for providing access to the C-band radar data and documentation in the framework of the INTERREG NWE RainGain project.

Author Contributions: Igor Paz wrote the paper; Ioulia Tchiguirinskaia, Daniel Schertzer and Bruno Tisserand conceived and designed the study; Ioulia Tchiguirinskaia and Daniel Schertzer collected the ENPC X-band radar data; Bernard Willinger gave access to the hydrological model; Igor Paz prepared the input data for the simulations; Bernard Willinger, Igor Paz, Auguste Gires and Laurent Monier performed the hydrological simulations; Igor Paz performed the multifractal analyses; Igor Paz, Auguste Gires, Ioulia Tchiguirinskaia and Daniel Schertzer analyzed all the results; Auguste Gires, Laurent Monier, Christophe Zobrist, Bruno Tisserand, Ioulia Tchiguirinskaia and Daniel Schertzer revised the paper.

Conflicts of Interest: The authors declare no conflict of interest.

References

1. Loukas, A.; Llasat, M.-C.; Ulbrich, U. Preface: "Extreme events induced by weather and climate change: evaluation, forecasting and proactive planning". *Nat. Hazards Earth Syst. Sci.* **2010**, *10*, 1895–1897, doi:10.5194/nhess-10-1895-2010.
2. WMO. Guide to Meteorological Instruments and Methods of Observation WMO-No. 8, 2014. Available online: http://www.wmo.int/pages/prog/www/IMOP/CIMO-Guide.html (accessed on 14 February 2017).
3. National Research Council of the National Academies. *Urban meteorology: Forecasting, monitoring, and meeting users' need*; Natl. Acad. Press: Washington, USA, 2012.
4. SIAVB. Available online: http://www.siavb.fr/riviere.aspx (accessed on 4 November 2016).
5. Diss, S.; Testud, J.; Lavabre, J.; Ribstein, P.; Moreau, E.; Parent du Chatelet, J. Ability of a dual polarized X-band radar to estimate rainfall. *Adv. Water Resour.* **2009**, *32 (7)*, 975–985.
6. Tabary, P.; Boumahmoud, A.-A.; Andrieu, H.; Thompson, R. J.; Illingworth, A. J.; Le Bouar, E.; Testud, J. Evaluation of two "integrated" polarimetric Quantitative Precipitation Estimation (QPE) algorithms at C-band. *J. Hydrol.* **2011**, *405 (3-4)*, 248–260, ISSN 0022-1694.
7. Emmanuel, I.; Andrieu, H.; Tabary, P. Evaluation of the new French operational weather radar product for the field of urban hydrology. *Atmos. Res.* **2012**, *103*, 20–32.
8. Figueras i Ventura, J.; Boumahmoud, A.-A.; Fradon, B.; Dupuy, P.; Tabary, P. Long-term monitoring of French polarimetric radar data quality and evaluation of several polarimetric quantitative precipitation estimators in ideal conditions for operational implementation at C-band. *Q. J. R. Meteorol. Soc.* **2012**, *138*, 2212–2228, doi:10.1002/qj.1934.
9. Figueras i Ventura, J.; Tabary, P. The New French Operational Polarimetric Radar Rainfall Rate Product. *J. Appl. Meteor. Climatol.* **2013**, *52*, 1817–1835.
10. Tabary, P. The new French operational radar rainfall product, Part I: Methodology. *Weather Forecast* **2007**, *22*, 393–408.
11. Ciach, G.J.; Habib, E.; Krajewski, W.F. Zero-covariance hypothesis in the error variance separation method of radar rainfall verification. *Adv. Water Resour.* **2003**, *26* (5), 573–580.
12. Gires, A.; Tchiguirinskaia, I.; Schertzer, D.; Schellart, A.; Berne, A.; Lovejoy, S. Influence of small scale rainfall variability on standard comparison tools between radar and rain gauge data. *Atmos. Res.* **2014**, *138*, 125–138.
13. Wyss, J.; Williams, E.R.; Bras, R.L. Hydrologic modeling of New England river basins using radar rainfall data. *J. Geophys. Res.* **1990**, *95 (D3)*, 2143–2152, doi:10.1029/JD095iD03p02143.
14. Sun, X.; Mein, R.G.; Keenan, T.D.; Elliot, J.F. Flood estimation using radar and raingauge data. *J. Hydrol.* **2000**, *239*, 4–18.
15. Germann, U.; Berenguer, M.; Sempere-Torres, D.; Zappa, M. REAL – Ensemble radar precipitation estimation for hydrology in a mountainous region. *Q. J. R. Meteorol. Soc.* **2009**, *135*, 445–456, doi:10.1002/qj.375.
16. Lobligeois, F. Mieux connaître la distribution spatiale des pluies améliore-t-il la modélisation des crues? Diagnostic sur 181 bassins versants français. PhD Thesis, Agro ParisTech, Paris, France, 2014.
17. Einfalt, T.; Denoeux, T.; Jacquet, G. A radar rainfall forecasting method designed for hydrological purposes. *J. Hydrol.* **1990**, *114 (3–4)*, 229–244.
18. Vieux, B. E.; Bedient, P.B. Assessing urban hydrologic prediction accuracy through event reconstruction. *J. Hydrol.* **2004**, *299*, 217–236.
19. Einfalt, T.; Arnbjerg-Nielsen, K.; Golz, C.; Jensen, N.-E.; Quirmbach, M.; Vaes, G.; Vieux, B. Towards a roadmap for use of radar rainfall data in urban drainage. *J. Hydrol.* **2004**, *299 (3–4)*, 186–202.

20. Berenguer, M.; Corral, C.; Sánchez-Diezma, R.; Sempere-Torres, D. Hydrological Validation of a Radar-Based Nowcasting Technique. *J. Hydrometeor.* **2005**, *6*, 532–549, doi: 10.1175/JHM433.1.
21. Liguori, S.; Rico-Ramirez, M.A.; Schellart, A.N.A.; Saul, A.J. Using probabilistic radar rainfall nowcasts and NWP forecasts for flow prediction in urban catchments. *Atmos. Res.* **2012**, *103*, 80–95, ISSN 0169-8095, http://dx.doi.org/10.1016/j.atmosres.2011.05.004.
22. Ichiba, A. X-band radar data and predictive management in urban hydrology. PhD Thesis, Université Paris-Est, Paris, France, 2016.
23. Peleg, N.; Blumensaat, F.; Molnar, P.; Fatichi, S.; Burlando, P. Partitioning the impacts of spatial and climatological rainfall variability in urban drainage modeling. *Hydrol. Earth Syst. Sci.* **2017**, *21*, 1559–1572, doi:10.5194/hess-21-1559-2017.
24. Schilling, W. Rainfall data for urban hydrology: what do we need? *Atmos. Res.* **1991**, *27*, 5–21.
25. Aronica, G.; Cannarozzo, M. Studying the hydrological response of urban catchments using a semi-distributed linear non-linear model. *J. Hydrol.* **2000**, *238 (1–2)*, 35–43.
26. Berne, A.; Delrieu, G.; Creutin, J.-D.; Obled, C. Temporal and spatial resolution of rainfall measurements required for urban hydrology. *J. Hydrol.* **2004**, *299*, 166- 179.
27. Segond, M.L.; Neokleous, N.; Makropoulos, C.; Onof, C.; Maksimović, Č. Simulation and spatio-temporal disaggregation of multi-site rainfall data for urban drainage applications. *Hydrol. Sci. J. – J. Des Sci. Hydrol.* **2007**, *52 (5)*, 917–935.
28. Schellart, A.N.A.; Shepherd, W.J.; Saul, A.J. Influence of rainfall estimation error and spatial variability on sewer flow prediction at a small urban scale. *Adv. Water Resour.* **2012**, *45*, 65–75.
29. Gires, A.; Onof, C.; Maksimović, Č.; Schertzer, D.; Tchiguirinskaia, I.; Simoes, N. Quantifying the impact of small scale unmeasured rainfall variability on urban runoff through multifractal downscaling: a case study. *J. Hydrol.* **2012**, *442*, 117–128.
30. Ochoa-Rodriguez, S.; Wang, L.-P.; Gires, A.; Pina, R.D.; Reinoso-Rondinel, R.; Bruni, G.; Ichiba, A.; Gaitan, S.; Cristiano, E.; van Assel, J.; Kroll, S.; Murlà-Tuyls, D.; Tisserand, B.; Schertzer, D.; Tchiguirinskaia, I.; Onof, C.; Willems, P.; ten Veldhuis, M.-C. Impact of spatial and temporal resolution of rainfall inputs on urban hydrodynamic modeling outputs: A multi-catchment investigation. *J. Hydrol.* **2015**, *531*, 389–407.
31. Simões, N.E.; Ochoa-Rodriguez, S.; Wang, L.-P.; Pina, R.D.; Marques, A.S.; Onof, C.; Leitão, J.P. Stochastic Urban Pluvial Flood Hazard Maps Based upon a Spatial-Temporal Rainfall Generator. *Water* **2015**, *7*, 3396, doi:10.3390/w7073396.
32. Gires, A.; Giangola-Murzyn, A.; Abbes, J.-B.; Tchiguirinskaia, I.; Schertzer, D.; Lovejoy, S. Impacts of small scale rainfall variability in urban areas: a case study with 1D and 1D/2D hydrological models in a multifractal framework. *Urban Water J.* **2014**, *12 (8)*, 607–617.
33. El-Tabach, E., Tchiguirinskaia, I.; Mahmood, O.; Schertzer, D. Multi-Hydro: a spatially distributed numerical model to assess and manage runoff processes in peri-urban watersheds. Final Conference of the COST Action C22, Road map towards a flood resilient urban environment; Pascheet, E., Evelpidou, N., Zevenbergen, C., Ashley, R., Garvin, S., Eds.; Paris, France, Hamburger Wasserbau-Schriftien, 2009.
34. Fewtrell, T.J.; Duncan, A.; Sampson, C.C.; Neal, J.C.; Bates, P.D. Benchmarking urban flood models of varying complexity and scale using high resolution terrestrial LiDAR data. *Phys. Chem. Earth* **2011**, Parts A/B/C, *36 (7–8)*, 281–291.
35. Giangola-Murzyn, A., Gires, A.; Hoang, C.T.; Tchiguirinskaia, I.; Schertzer, D. Multi-Hydro modelling to assess flood resilience across scales, case study in the Paris region. 9th International Conference on Urban Drainage Modelling; Belgrade, Serbia, 2012.
36. Tramblay, Y.; Bouvier, C.; Crespy, A.; Marchandise, A. Improvement of flash flood modelling using spatial patterns of rainfall: a case study in southern France, Proceedings of the Sixth World FRIEND Conference; IAHS Publ., Fez, Morocco, 2010; 340.
37. RainGain Project. Available online: www.raingain.eu (accessed on 21 July 2016).
38. Schertzer, D.; Tchiguirinskaia, I.; Lovejoy, S.; Hubert, P. No monsters, no miracles: in nonlinear sciences hydrology is not an outlier! *Hydrolog. Sci. J.* **2010**, *55 (6)*, 965 — 979.
39. Réseau hydrographique. Available online: https://www.data.gouv.fr/fr/datasets/reseau-hydrographique-idf/ (accessed on 14 December 2015).
40. Wallingford Software. InfoWorks CS Help Documentation, 2009.
41. Marshall, J.S.; Palmer, W.M. The distribution of raindrop with size. *J. Meteor.* **1948**, *5*, 165-166.

Preprints (www.preprints.org) | NOT PEER-REVIEWED | Posted: 14 October 2017 doi:10.20944/preprints201710.0096.v1

42. Parent du Châtelet, J. ARAMIS, le réseau Français de radars pour la surveillance des précipitations. *La Météorologie* **2003**, *40*, 44–52.
43. Gourley, J.J.; Tabary, P.; Parent du Chatelet, J. A fuzzy logic algorithm for the separation of precipitating from nonprecipitating echoes using polarimetric radar observations. *J. Atmos. Ocean. Tech.* **2007**, *24(0)*, 1439–1451.
44. Selex. Selex METEOR manual, 2015.
45. Fulton, R.A.; Bredienbach, J.P.; Seo, D.-J.; Miller, D.A.; O'Bannon, T. The WSR-88 rainfall algorithm. *Weather Forecasting* **1998**, *13*, 377–395.
46. Matrosov, S.Y.; Clark, K.A.; Martner, B.E.; Tokay, A. X-Band Polarimetric Radar Measurements of Rainfall. *J. Appl. Meteor.* **2002**, *41*, 941–952, doi:10.1175/1520-0450(2002)041<0941:XBPRMO>2.0.CO;2.
47. Schertzer, D.; Lovejoy, S. Physical modeling and Analysis of Rain and Clouds by Anisotropic Scaling Multiplicative Processes. *J. Geophys. Res.* **1987**, *D 8 (8)*, 9693–9714.
48. Gupta, V.K.; Waymire, E. A Statistical Analysis of Mesoscale Rainfall as a Random Cascade. *J. Appl. Meteorol.* **1993**, *32*, 251–267.
49. Harris, D.; Menabde, M.; Seed, A.; Austin, G. Multifractal characterization of rain fields with a strong orographic influence. *J. Geophys. Res.* **1996**, *101*, 26,405-26,414.
50. Marsan, D., Schertzer, D.; Lovejoy, S. Causal space-time multifractal processes: Predictability and forecasting of rain fields. *J. Geophys. Res.* **1996**, *101 (D21)*, 26,333–26,346.
51. Olsson, J.; Niemczynowicz, J. Multifractal analysis of daily spatial rainfall distributions. *J. Hydrol.* **1996**, *187*, 29-43.
52. de Lima, M.I.P.; Grasman, J. Multifractal analysis of 15-min and daily rainfall from a semi-arid region in Portugal. *J. Hydrol.* **1999**, *220 (1-2)*, 1–11.
53. Deidda, R. Rainfall downscaling in a space-time multifractal framework. *Water Resour. Res. 2000*, *36*, 1779–1794.
54. Pathirana, A.; Herath, S. Multifractal modeling and simulation of rain fields exhibiting spatial heterogeneity. *Hydrol. Earth Syst. Sci.* **2002,** *6*, 695–708.
55. Biaou, A.; Hubert, P.; Schertzer, D.; Tchiguirinskaia, I.; Bendjoudi, H. Fractals, multifractals et prévision des précipitations. *Sud Sciences et* Technologies **2003**, *10*, 10–15.
56. Pathirana, A.; Herath, S.; Yamada, T. On the modeling of temporal correlations in spatial-cascade rainfall downscaling. In *Weather radar information and distributed hydrological modeling*; Tachikawa, Y., Vieux, B.E., Georgakakos, K.P., Nakakita, E., Eds.; IAHS Publication, 282, 74–82.
57. Ferraris, L.; Gabellani, S.; Parodi, U.; Rebora, N.; von Hardenberg, J.; Provenzale, A. Revisiting multifractality in rainfall fields. *J. Hydrometeorol.* **2003**, *4*, 544–551.
58. Ferraris, L.; Gabellani, S.; Rebora, N.; Provenzale, A. A comparison of stochastic models for spatial rainfall downscaling. *Water Resour. Res.* **2003**, *39*, 1368-1384.
59. Macor, J.; Schertzer, D.; Lovejoy, S. Multifractal Methods Applied to Rain Forecast Using Radar Data. *La Houille Blanche* **2007**, *4*, 92–98.
60. Royer, J.F.; Biaou, A.; Chauvin, F.; Schertzer, D.; Lovejoy, S. Multifractal analysis of the evolution of simulated precipitation over France in a climate scenario. *C. R. Geosci.* **2008**, *340*, 431–440.
61. Nykanen, D.K. Linkages between Orographic Forcing and the Scaling Properties of Convective Rainfall in Mountainous Regions. *J. Hydrometeorol.* **2008**, *9*, 327–347.
62. De Montera, L.; Barthes, L.; Mallet, C.; Gole, P. The effect of rain-no rain intermittency on the estimation of the universal multifractals model parameters. *J. Hydrometeorol.* **2009**, *10*, 493–506.
63. Langousis, A.; Veneziano, D.; Furcolo, P.; Lepore, C. Multifractal rainfall extremes: Theoretical analysis and practical estimation**.** *Chaos, Solitons & Fractals* **2009**, *39*, 1182-1194, doi:10.1016/j.chaos.2007.06.004.
64. Tchiguirinskaia, I.; Schertzer, D.; Hoang, C.-T.; Lovejoy, S. Multifractal study of three storms with different dynamics over the Paris region, Proceedings of Weather Radar and Hydrology; Moore, J., Cole, S., Illingworth, A., Eds.; IAHS Publ., Exeter, United Kingdom, 2011, 351, 421–426.
65. Hoang, C.-T.; Tchiguirinskaia, I.; Schertzer, D.; Lovejoy, S. Caractéristiques multifractales et extrêmes de la précipitation à haute resolution, application à la détection du changement climatique. *Revue des Sciences de l'Eau – Journal of Water Science* **2014**, *27 (3)*, 205–216, doi: 10.7202/1027806ar.
66. Schertzer, D.; Lovejoy, S. Universal Multifractals do Exist! *J. Appl. Meteorol.* **1997**, *36*, 1296–1303.
67. Schertzer, D.; Lovejoy, S. Multifractals, generalized scale invariance and complexity in geophysics. *Int. J. Bifurcat. Chaos* **2011**, *21*, 3417–3456.

Preprints (www.preprints.org) | NOT PEER-REVIEWED | Posted: 14 October 2017 doi:10.20944/preprints201710.0096.v1

68. Lavallée, D.; Lovejoy, S.; Ladoy, P. Nonlinear variability and landscape topography: analysis and simulation. In *Fractals in geography*; De Cola, L., Lam, N., Eds.; Prentice-Hall, 1993; 171–205.